# **ENVIRONMENTAL RESEARCH**

**LETTERS** 



### **OPEN ACCESS**

#### RECEIVED

6 September 2020

#### REVISED

18 November 2020

## ACCEPTED FOR PUBLICATION

24 November 2020

#### PUBLISHED

23 December 2020

Original content from this work may be used under the terms of the Creative Commons Attribution 4.0 licence.

Any further distribution of this work must maintain attribution to the author(s) and the title of the work, journal citation and DOI.



## **LETTER**

# Formation and dissipation dynamics of the Asian tropopause aerosol layer

Qianshan He<sup>1,2</sup>, Jianzhong Ma<sup>3</sup>, Xiangdong Zheng<sup>3</sup>, Yanyu Wang<sup>4</sup>, Yuhang Wang<sup>5</sup>, Haizhen Mu<sup>2</sup>, Tiantao Cheng<sup>4</sup>, Ruilian He<sup>6</sup>, Guan Huang<sup>7</sup>, Dongwei Liu<sup>2</sup> and Jos Lelieveld<sup>8</sup>

- Shanghai Meteorological Service, Shanghai, People's Republic of China
- <sup>2</sup> Shanghai Key Laboratory of Meteorology and Health, Shanghai, People's Republic of China
- <sup>3</sup> State Key Laboratory of Severe Weather and CMA Key Laboratory of Atmospheric Chemistry, Chinese Academy of Meteorological Sciences, Beijing, People's Republic of China
- Department of Atmospheric and Oceanic Sciences and Institute of Atmospheric Sciences, Fudan University, Shanghai, People's Republic of China
- Georgia Institute of Technology, Atlanta, GA, United States of America
- <sup>6</sup> Key Laboratory of Meteorological Disaster, Ministry of Education (KLME)/Joint International Research Laboratory of Climate and Environment Change (ILCEC), Nanjing University of Information Science and Technology, Nanjing, People's Republic of China
- College of Environmental Science and Engineering, Donghua University, Shanghai, People's Republic of China
- <sup>8</sup> Max Planck Institute for Chemistry, Mainz, Germany

E-mail: majz@cma.gov.cn

**Keywords:** ATAL, ASM, QBO, CALIPSO, dynamics Supplementary material for this article is available online

# **Abstract**

The Asian tropopause aerosol layer (ATAL) is characterized by enhanced aerosol concentrations in the Asian summer monsoon anticyclone in the upper troposphere and lower stratosphere at 13–18 km altitude. A growing body of evidence suggests that the aerosol enhancement is closely connected with deep convection during the monsoon. However, the origin of the aerosols is under debate, and the key factors that determine the ATAL variability remain poorly understood. We investigated the formation and dissipation mechanisms of the ATAL and the inter-annual variation from a dynamical viewpoint using satellite observations and meteorological reanalysis data from 2012 to 2018. We identified the northern Bay of Bengal and adjacent land area, where air pollution from the Indian subcontinent converges, as the major convection source area of aerosols to the ATAL. The spatial extent of the ATAL, represented by the mean attenuated scattering ratio from satellite measurements, appears to be related to a secondary circulation driven by the stratospheric quasi-biennial oscillation. The aerosols are not homogeneously distributed within the ATAL, and descending motion in the western part is found to play an important role in dissipation of the layer. These findings elucidate the ATAL dynamics and associated regional and global air pollution transports.

# 1. Introduction

The Asian tropopause aerosol layer (ATAL, more information about acronyms, abbreviations and definitions can be found in supplementary file) is characterized by enhanced aerosol extinction extending horizontally from the Eastern Mediterranean across India to Western China ( $\sim 5-105^{\circ}$  E;  $\sim 15-45^{\circ}$  N) and vertically from about 13 km to 18 km altitude, and it forms in May/June with the onset of the Asian summer monsoon (ASM), while it dissipates around September with the breakup of the ASM associated

anticyclonic circulation (Vernier *et al* 2011, 2015, Thomason and Vernier 2013). Air pollution in the ATAL causes a significant regional radiative forcing (RF), and is important for the aerosol loading of the global stratosphere, which significantly influences climate change (Vernier *et al* 2015, Yu *et al* 2017).

The ASM induces quasi-stationary anticyclonic circulation, located in the upper troposphere and lower stratosphere (UTLS) over Asia and the Middle East during boreal summer and flanked by the subtropical westerly jet to the north and the equatorial easterly jet to the south (Li *et al* 2005, Fu *et al* 2006,

Randel and Park 2006, Park et al 2007, 2008, 2009, Randel et al 2010). The appearance of the ASM is mainly connected with the seasonal shifts of the Intertropical Convergence Zone, land-ocean thermal contrasts (Basha et al 2020), and also the diabatic heating associated with persistent deep convection, which results in rapid vertical transport of near-surface air from Southeast and South Asia and confinement of the air masses by the strong anticyclone during summer (Hoskins and Rodwell 1995, Highwood and Hoskins 1998). The mean upward circulation, especially at the eastern side of the anticyclone extends the transport into the lower stratosphere. The ASM offers a transport pathway of anthropogenic pollutants like carbon monoxide (CO) and hydrogen cyanide (HCN) as well as water vapor from the boundary layer into the UTLS through convective overshooting and into the stratospheric Brewer-Dobson circulation (Gettelman et al 2004, Fu et al 2006, Fueglistaler et al 2009, Randel et al 2010, Bian et al 2011, Srivastava et al 2016). Previous studies have concluded that deep convection can efficiently transport aerosols and their precursors from the boundary layer into the interior of the anticyclone, where they can be trapped for several months, subject to slow, largescale ascent and weak lateral exchange with air masses outside the anticyclone (Dethof et al 1999, Randel and Park 2006). However, if the polluted air would be fully confined in the interior of the anticyclone with continuous intrusions of fresh aerosols and gaseous precursors, the ATAL intensity would increase ceaselessly throughout the ASM period, from the onset until the breakup of the associated anticyclonic circulation. But in fact, the ATAL intensity remains approximately constant during the ASM period. Therefore, we expect mechanisms which play a role in maintaining the balance of the ATAL intensity throughout the ASM period.

Deep convection occurs in different areas within the ASM region, most frequently over the Bay of Bengal (BoB), North India, the South China Sea, the Southern Tibetan Plateau (TP), and the central TP (Fu et al 2006, Tzella and Legras 2011, Wright et al 2011, Bergman et al 2012, 2013). A study by Chen et al (2012), based on Lagrangian model simulations driven by Global Forecast System wind fields, suggested that transport from the boundary layer to the UTLS is predominant over the Western Pacific region and the South China Sea, followed by the BoB and the South Asian subcontinent and, to a lesser extent, the TP. A few studies argued that the main air source within the ASM anticyclone is from the Indian subcontinent (Bergman et al 2013, Yan and Bian 2015, Lelieveld et al 2018). The TP is located at the core region of the ASM, thereby potentially acting as a significant transport pathway for pollutants to enter the stratosphere (Fu et al 2006, Wright et al 2011, Bergman et al 2013, Gu et al 2016). The formation of the ATAL is multi-facetted, as it

involves not only dynamics (and deep convection) but also chemical (e.g. for secondary aerosols) and deposition processes, depending on environmental conditions (e.g. temperature and relative humidity) and geographical regions in which important emission sources of pollutants are located (both for aerosols and their gaseous precursors). Therefore, trajectory analysis without considering aerosol sources and sinks may not fully capture the transport of surface sources into the ATAL.

Atmospheric chemistry general circulation models have been used to simulate the formation of the ATAL (Li et al 2005, Fadnavis et al 2013, Neely et al 2014, Yu et al 2015, Gu et al 2016, Lelieveld et al 2018, Ma et al 2019). Although all models could predict the general contours of the ATAL (i.e. enhancement of aerosols at the tropopause within the ASM anticyclone), there is controversy among the model analyses about the chemical components that dominate the ATAL and the most important emission sources. Vernier et al (2015) reported that the aerosol optical depth (AOD) of the ATAL had increased by a factor of three from the late 1990s to the early 2000s, exerting a short-term direct regional RF of  $-0.1 \text{ W m}^{-2}$  at the top of atmosphere over 18 years, comparable but of different sign as the total RF due to increased carbon dioxide (CO<sub>2</sub>) over the same period. Note that Vernier et al (2015) calculated the RF based on the assumption that the ATAL was composed of sulfate and organic aerosols (OAs), while recent balloon measurements showed that nitrate was an important component of the ATAL while sulfate was below the detection limit (Vernier et al 2018). It should be noted that increased sulfur dioxide (SO<sub>2</sub>) emissions in India, as reported by recent studies (e.g. Krotkov et al 2016), cannot fully explain the trend of the ATAL. In addition to increasing emission sources, inter-annual changes in dynamic features associated with the ASM may influence the ATAL intensity (Lau et al 2018, Yuan et al 2019, Bian et al 2020).

The ASM is subject to strong dynamic variability, oscillations and eddy shedding (e.g. Randel and Park 2006, Yan et al 2011, Pokhrel et al 2012, Garny and Randel 2013, Vogel et al 2014, Nützel et al 2016, Luo et al 2018). Inter-annual dynamical processes such as the quasi-biennial oscillation (QBO) can play a role in transporting trace gases and aerosols from the surface to the UTLS (Garny and Randel 2016, Pan et al 2016). The QBO, known to modulate tropical convection (Collimore et al 2003, Fadnavis et al 2013, Nie and Sobel 2015), consists of a primary circulation with alternating easterly-westerly stratospheric winds descending from about 30 km to the tropopause with a period of about 26–27 months (Baldwin et al 2001). Although the QBO is confined to the tropics, the oscillation can induce secondary circulations in the extra-tropics and affect the temperate latitudes through changes in planetary wave ducting. Previous research focused on the influence of the QBO on the transport of trace gases and aerosols from the surface to the UTLS in the tropics (e.g. Collimore *et al* 2003, Schoeberl *et al* 2008, Ding and Fu 2018). No work has yet been reported to quantify the relation of the interannual QBO variability with the ATAL intensity in the ASM region. In this study we fill the gap with the help of long-term records of the QBO together with atmospheric vertical motion from the most recent ERA5 reanalysis data and the attenuated scattering ratio (ASR) from the Cloud-Aerosol Lidar and Infrared Pathfinder Satellite Observations (CALIPSO) stratospheric aerosol product for the ASM region. We also investigated the potential mechanisms that balance the ATAL intensity against vertical transport by deep convection during the ASM period.

# 2. Data

The CALIPSO satellite is part of the A-train constellation, which was launched in April 2006 to a Sun Synchronous polar orbit with 98.2° inclination at an altitude of 705 km (Winker et al 2009). The constellation repeats the cycle every 16 d with local equator crossing times of nearly 01:30 h and 13:30 h (Winker et al 2009). The Cloud-Aerosol Lidar with Orthogonal Polarization (CALIOP) is one of the main instruments on board the CALIPSO satellite with a dual-wavelengths (532 nm and 1064 nm) polarization sensitive lidar. CALIOP provides profiles of clouds and aerosols and is capable of detecting clouds with an optical depth of 0.01 or less. Because of the low levels of aerosols in the UTLS region during non-volcanic periods, features of the ATAL could not be clearly detected by the L2 products of the extinction coefficient, nor by their vertical integral referred to as AOD. We utilized L3 global distribution of monthly gridded stratospheric aerosol profile data of 532 nm ASR (https://eosweb.larc.nasa.gov/project/calipso/cal\_ lid\_l3\_stratospheric\_apro-standard\_v1-00) to investigate the distribution and intensity of ATAL from 2012 to 2018. In this data product, ASR is computed using equation (1):

$$ASR = \beta \prime / (\beta_{\rm m} \times T^2_{\rm m} \times T^2_{O3}) \tag{1}$$

where  $\beta'$  is the L1B attenuated backscatter.  $T^2{}_{\rm m}$  and  $T^2{}_{\rm O3}$  refer to the two-way transmittance from the molecules and that of ozone respectively and  $\beta_{\rm m}$  is the modeled molecular backscatter coefficient.  $T^2{}_{\rm m}$  and  $T^2{}_{\rm O3}$  are computed from the meteorological model (MERRA-2) used for CALIOP V4.10 data products.

This profile dataset is available on a monthly basis with 900 m vertical resolution from 8.2 km to 36.2 km and 20° longitude by 5° latitude horizontal resolution. The ASR averaged in the range of 13–18 km is used to represent the intensity of ATAL. Specifically, the data with high noise is discarded. Outliers are eliminated using a spike filter that uses a threshold

scheme similar to the one used in the automatic layer detection scheme in the CALIOP L2 algorithm (Vaughan *et al* 2009).

We also utilized the L3 global distribution of monthly gridded tropospheric aerosol profile data of 532 nm extinction coefficient (https://eosweb.larc.nasa.gov/project/calipso/cal\_ lid\_13\_tropospheric\_apro\_cloudfree-standard-V4-20) to investigate the transportation and linkage of tropospheric aerosol to the ATAL. The version 4.20 release of the CALIPSO lidar L3 tropospheric aerosol profile product was released in September 2019. The new L3 product is constructed from version 4 L2 input data which are the highest quality and most sophisticated of all CALIOP L2 data products. New L3 quality screening procedures have been implemented to improve the quality of statistics reported by the product. This profile data has a 60 m vertical resolution from 0 km to 12 km and horizontal resolution of  $2^{\circ}$  latitude by  $5^{\circ}$  longitude.

The L3 MODIS Atmosphere Monthly Global Product MOD08\_M3 (https://atmosphere-imager.gsfc.nasa.gov/products/) is used to investigate the AOD variation in the ASM region. The monthly dataset involves the AOD over both land and ocean with a horizontal resolution of 1° latitude by 1° longitude.

The most recent ERA5 reanalysis, which was released by the European Centre for Medium-Range Weather Forecasts (ECMWF) in 2018, has been used. Compared to ERA-Interim (Dee et al 2011), the ERA5 data assimilation system uses the new version of the Integrated Forecasting System (IFS Cycle 41r2) instead of IFS Cycle 31r2 by ERA-Interim. In addition, various newly reprocessed data sets, recent instruments, cell pressure correction stratospheric sounding units, improved bias correction for radiosondes, etc, are updated in ERA5. Ming et al (2019) evaluated the representation of temperature and ozone in the UTLS and concluded that ERA5 is significantly improved compared to ERA-Interim by better agreement with the Global Navigation Satellite System radio occultation (GNSS RO) temperature. The monthly meteorological fields contained in the ERA5 data are available on 60 hybrid model levels from the ground to 0.1 hPa at a spatial resolution of  $2.5^{\circ} \times 2.5^{\circ}$ . The geopotential height, temperature, specific humidity and horizontal wind at the 100 hPa level as well as vertical velocity at 37 pressure levels from 1000 hPa to 1 hPa are selected in this study. The ASM intensity index (ASMI) is defined as follows (Webster and Yang 1992),

$$ASMI = U_{100} - U_{500} \tag{2}$$

where U is the regionally averaged monthly zonal wind at the corresponding barometric surface, indicated as subscript over the domain  $(40-110^{\circ} \text{ E}, 0-40^{\circ} \text{ N})$ . A higher ASMI refers to

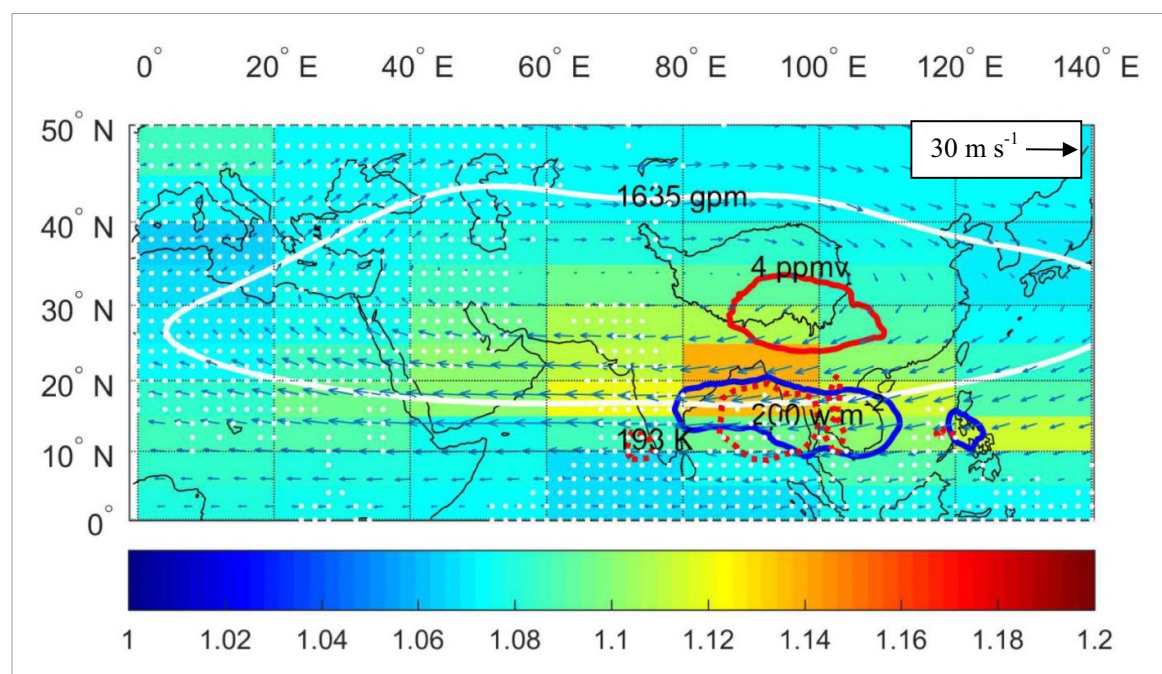


**Figure 1.** The climatological distribution of mean attenuated scattering ratio (ASR) in the upper troposphere and lower stratosphere (UTLS, at an altitude range of 13–18 km) during the entire Asian summer monsoon (ASM) period from 2012 to 2018 (color shading), superimposed with wind vectors and the contours of geopotential height at 1635 gpm (white solid line), temperature at 194 K (blue solid line), water vapor at 4 ppmv (red solid line) and outgoing long-wave radiation (OLR) at  $200 \text{ w m}^{-2}$  (dashed contours) at 100 hPa. Locations with vertical motion  $>0 \text{ Pa s}^{-1}$  (indicating descent) are highlighted with white dots. The coastline and outline of the TP are also indicated with black thin solid lines. A reference wind vector (30 m s<sup>-1</sup>) is shown in upper right corner.

stronger vertical wind shear and enhanced monsoon circulation.

The outgoing long-wave radiation (OLR) averaged over this region is an indicator of convective forcing; hence the OLR time series can be used as a proxy of monsoon convection (Randel and Park 2006). NOAA interpolated OLR at a spatial resolution of 2.5° × 2.5° is used as a proxy for convection. This data was downloaded from https://www.esrl.noaa.gov/psd/data/gridded/data.interp\_OLR.html.

For the QBO, we used the normalized monthly mean zonal winds (m s<sup>-1</sup>) at 30 hPa level over Singapore (1° N, 104° E) as QBO index. This data set is available at https://www.geo.fuberlin.de/met/ag/strat/produkte/qbo.

Topography information is provided by the Global Multi-resolution Terrain Elevation Data 2010 (GMTED2010) website (https://www.temis.nl/data/gmted2010/) of the U.S. Geological Survey (USGS) and the U.S. National Geospatial-Intelligence Agency (NGA).

# 3. Results and discussion

Figure 1 shows the distribution of mean ASR in the UTLS and associated meteorological variables at 100 hPa during the ASM period for the years 2012–2018. It shows the pronounced mean anticyclonic (high pressure) and water vapor center in the UTLS, with strong easterlies in the tropics and westerlies

in the extra-tropics, in conjunction with a cold center over the southern TP. Significant deep convection occurs over the west coast of India, BoB, northeastern India, and occasionally over the southern TP. These are well-known climatological features associated with the ASM (Lau and Li 1984, Krishnamurti 1985, Yanai et al 1992, Webster et al 1998, Wu et al 2007). Pronounced enhancement in ASR with a magnitude ranging from 1.05 to 1.22 is found over the southern anticyclone, spanning the Arabian Peninsula, the Himalayan-Gangetic Plain (HGP) and the China South Sea, with the highest ASR appearing over the northern BoB, East India and Bangladesh. The regions with the maximum ASR largely overlap with those of the minimum tropopause temperature and deep convection, with the former being located to the north of the latter, where pollutants from nearby emission sources are abundant and can be transported upward by deep convection associated with the ASM (Randel et al 2015). The most noteworthy aspect of the ASR is the confined local maximum over the BoB.

Note that in most years, except for 2012 and 2018, the ASR and deep convection maxima show notable differences with respect to the horizontal locations. The pronounced ASR enhancement is located north of the deep convection region. There is a pattern of strong enhancement of ASR between 15–25° N and 80–100° E, just over the northern BoB and Bangladesh, located at the northwestern edge of the extensive areas of the strongest convection.

Compared to southeastern Asia and central India, higher AODs are found around the northern BoB and adjacent coastal areas (figure S2 (available online at https://stacks.iop.org/ERL/16/014015/mmedia)), where strong convection occurs as well. Therefore, the locations of largest aerosol loading in the planetary boundary layer (PBL) and deep convection indicate that the major pathway for the convective transport of aerosols and precursors to the tropopause is located at the northern BoB and adjacent land areas. The deep convection over the BoB triggers low-level convergence of polluted air from the Indian subcontinent. It appears that the aerosols transported to the UTLS over the northern BoB and adjacent land areas originate from anthropogenic sources since carbon monoxide, which is generally considered as a pollution tracer, takes on a similar regional distribution pattern (figure S3). Our results are in agreement with recent studies (e.g. Lau et al 2018, Lelieveld et al 2018) in that South Asia emissions are a major pollution source of the ATAL. However, there are inconsistences with respect to the specific regions over which deep convection can transport South Asian pollutants to the UTLS most efficiently. Lau et al (2018) proposed that the HGP in northern and northeastern India and the Sichuan Basin in southwestern China are the two preferred regions for vertical transport of CO, OAs, and dust to the ATAL. Note that in addition to OA and dust, the ATAL also contains nitrate, sulfate and other aerosols (He et al 2019, Höpfner et al 2019, Ma et al 2019), which are likely to have different source regions and physical properties (e.g. solubility) from those of CO, OA and dust. Moreover, there are remaining uncertainties in model simulations, even for the vertical transport pathway of dust to the UTLS during ASM (Lau et al 2018, Ma et al 2019, Yuan et al 2019). Our findings based on satellite data analysis provide an observational base for further model investigations.

As shown in figure S1, the enhancements of ASR in the UTLS during the ASM period show large interannual differences from 2012 to 2018, with the ASR varying from a minimum of 1.058 in 2013 to a maximum of 1.075 in 2012, averaged over the ATAL region (15-45° N; 5-105° E) defined by Vernier et al (2011, 2015). Since pollution emissions are not expected to be highly variable on an inter-annual basis, changes in the activity of deep convection are likely to be primarily responsible for the inter-annual variability in the ASR during the ASM period. It should be noted that the geographical location and range of strong anticyclonic circulation varied from year to year (see figure S1). The inter-annual variations in the intensity of the ATAL compared to that of the ASM were investigated based on the relationship between the regionally averaged ASR in the ATAL and the QBO index for different ASM periods (see figure 2). The inter-annual fluctuations in the ASR appear to be synchronized with inter-annual QBO index variations.

Higher ASR corresponds to the easterly shear (negative) phase of the QBO and the lower value matches the westerly (positive) phase. The highest ASR corresponds to the lowest QBO index in 2012, and vice versa in 2013. The ASR and QBO show an anti-phase relationship with a correlation coefficient of -0.78 (p=0.04 within a confidence level of 95%, same as hereafter). The ASM intensity is associated with the QBO, and the correlation coefficient between the QBO index and the ASMI was calculated to be as high as 0.91 (p=0.004) for the years 2012–2018 (see figure S4).

Previous work has shown that the QBO-induced secondary circulation is associated with an increase in upwelling during the easterly shear phase and a suppression of the upwelling during the westerly phase (Plumb and Bell 1982), and large anomalies of annual cycle variations in water vapor and other trace gases are due to the QBO disruption (Schoeberl et al 2008). The regionally averaged ASR in 2013, when the QBO index was in the westerly phase characterized by suppression of upwelling, is relatively lower than that in 2012, 2014 and 2018, when the negative QBO index was in the easterly shear phase. This result is consistent with the conclusion about the variation in water vapor during the 2015-2016 QBO disruption by Tweedy et al (2017). We also investigated the relationship between the regional average CO mixing ratio and the QBO index for different ASM periods, and the result also shows a correlation, although not as significant as that between the ASR and the QBO (figure 2). Atmospheric CO levels over South Asia are significantly influenced by biomass burning, and a close relationship between the CO mixing ratio in the UTLS region and the carbon emission flux from biomass burning is found (R = 0.79with p = 0.06, figure S5). The increasing trends of ASR with CO mixing ratio underscore the influence of anthropogenic pollution on the formation of the ATAL. As mentioned above, we applied the latitude and longitude range of 15-45° N and 5-105° E to average the ASRs over the ATAL region. Sensitivity tests show that small differences in selected latitude and longitude range does not substantially change the inverse relationship between the ASR and the QBO (see table S1).

The increase in tropopause ASR with decreasing QBO index can be attributed to dynamic processes, i.e. the intensification of the secondary circulation driven by the QBO. Figure 2 also shows that deep convective activity increases with decreasing QBO index, being strongest between 10° N and 20° N during the extreme easterly shear phase. Deep convective activity is gradually suppressed with an increasing QBO index. Collimore *et al* (2003) investigated the mechanisms linking the QBO with deep convection and found that the QBO modulation of tropopause height can allow convection to penetrate deeper. Therefore, deeper convection favors the

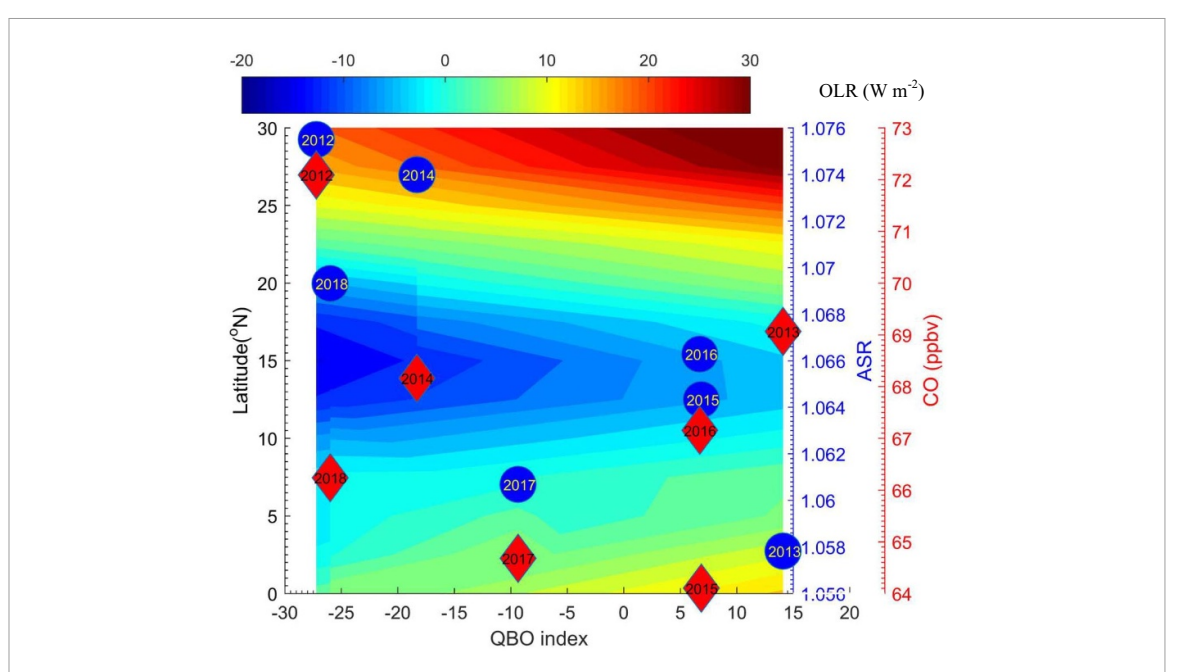


**Figure 2.** The relationship between the quasi-biennial oscillation (QBO) index and the average ASR enhancement in the ATAL (blue circles), as well as the average CO mixing ratio at 100 hPa in the ASM region (15–45 $^{\circ}$  N and 5–105 $^{\circ}$  E), and the variation of zonal mean anomalous OLR (W m $^{-2}$ ) in the convective regions (60–120 $^{\circ}$  E) at different latitudes with the QBO index during the ASM period, for the 7 years from 2012 to 2018.

transport of aerosols and gaseous precursors from the PBL to the tropopause. Some previous studies concluded that ENSO affects the ASM characterized by large anomalies in trace gases (ozone and CO) in the tropical UTLS region (e.g. Ravindrababu *et al* 2019). In this study, we have also analyzed the impact of ENSO on ASM and ASR, and found no significant relationship between them with R = 0.16.

We further explored the inter-annual variations of the three-dimensional structure of the vertical velocity with the QBO. The latitude-height cross sections of the vertical velocities and the difference between 2012 and 2013 at the 90° E cross section are shown in figure S6. These 2 years, characterized by the extreme QBO index during the easterly and westerly phase, respectively, are particularly suitable to demonstrate the difference in vertical velocity induced by the QBO secondary circulation. Three outstanding columns with stronger upwelling motion, reaching the UTLS and capped near 100-90 hPa, are identified at about 18° N, 25° N and 32° N during the easterly phase in the year 2012. This QBO-associated secondary circulation anomaly produces upwelling by -0.05 Pa s<sup>-1</sup> with a peak of -0.15 Pa s<sup>-1</sup> at the southern flank of the TP, which facilitates the entry of tropospheric constituents into the subtropical lower stratosphere. The increased subtropical upwelling also supports the transport of aerosols from the upper troposphere to the lower stratosphere. As found in previous studies (e.g. Fadnavis et al 2013, Nie and Sobel 2015), this upwelling develops in association with the QBOderived secondary circulation near the UTLS. Interestingly, the descending motion over the region north of the TP is suppressed during the easterly phase

of the QBO in 2012. This configuration of atmospheric vertical motion helps maintaining a balance of the ATAL intensity. The ASM anticyclone is generally isolated although horizontal exchanges can occur due to dynamical instabilities (Gottschaldt *et al* 2018). Chemical formation and transformation of aerosols can occur within the ASM due to enhanced hydroxyl (OH) radical and aerosol precursors concentrations (Höpfner *et al* 2016, 2019, Lelieveld *et al* 2018, Ma *et al* 2019, Lamotte *et al* 2020). Aerosols in the ATAL can undergo gravitational settling, which should not be a dominant sink for the small particles in the accumulation mode and which could be counteracted by large-scale upward motion in the eastern ATAL (Renard *et al* 2018).

A most striking feature of the ATAL is the asymmetry in the regional distribution of enhanced aerosol levels even within the anticyclone. Relatively high ASR on the southeast of the anticyclone coincides with the strong convection between 40° E to 120° E and 10° N to 30° N. To the west of this strong convection region, there is a gradual decrease of ASR associated with downward transport and westward advection from the hot spot over the BoB, where the largest enhancement of ASR has been found (see figure 1). We analyzed this asymmetry distribution of ASR together with the vertical velocity from the ERA5 data, and noticed that the spatial distribution of enhanced aerosol in the UTLS was closely related to the horizontal cycle and vertical motion. During the ASM period, westerlies and descending motion prevail over the Middle East and northeastern Africa (figure 1). This overlap between the main descent region and the low ASR indicates

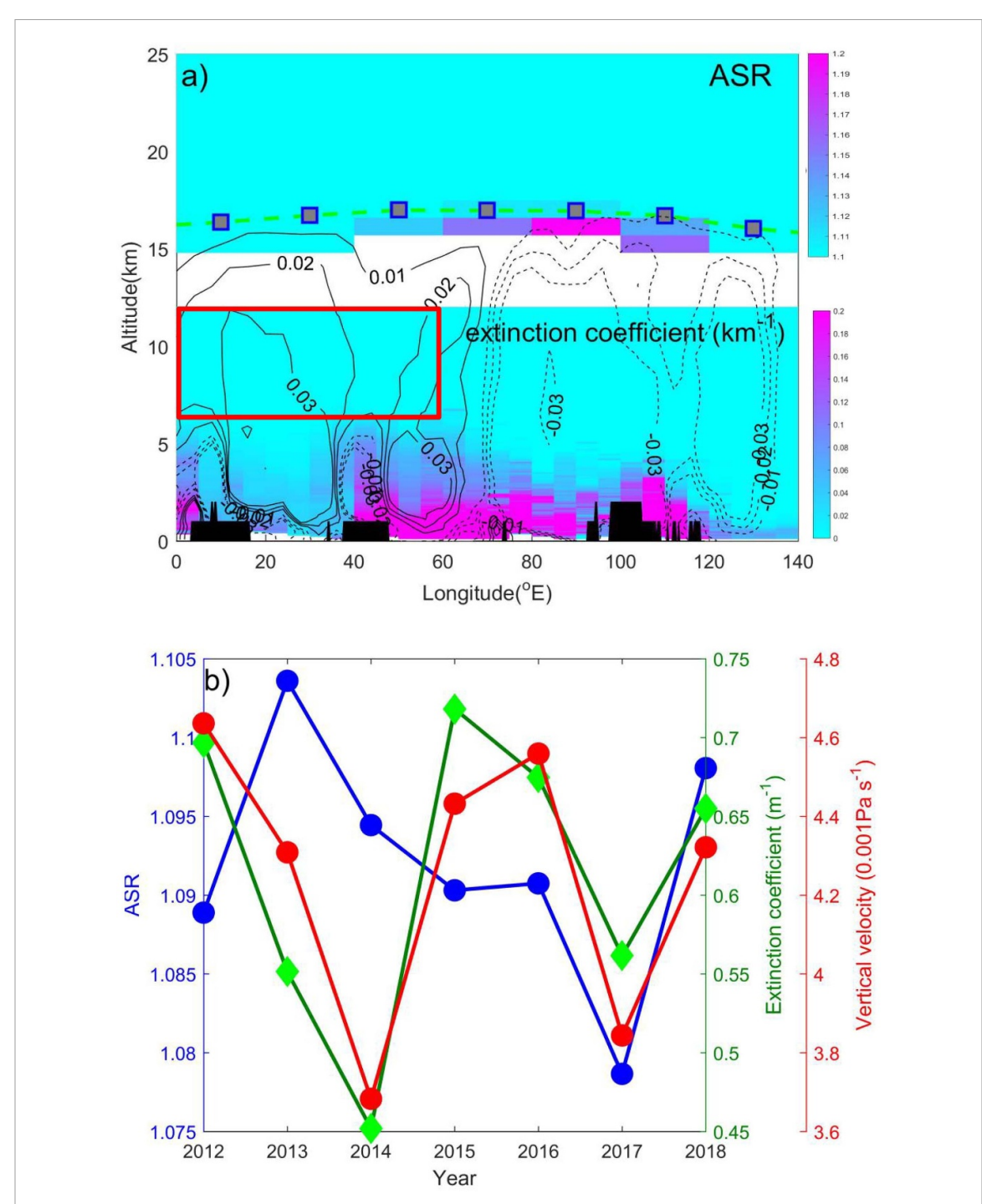


**Figure 3.** (a) Longitude–altitude cross section  $(0-140^{\circ} \text{ E})$  of the ASR and extinction coefficient over the equatorial easterly jet  $(25^{\circ} \text{ N})$  and associated vertical motion  $(\text{Pa s}^{-1})$  field with solid (dashed) contours indicating descent (ascent), averaged over the ASM period in 2012. The squares with green dashed lines denote the tropopause altitude derived from the CALIPSO satellite L3 monthly stratospheric aerosol data during the same period. The black areas denote the terrain height (km) above sea level. The red rectangle denotes the upper troposphere below the western Asian tropopause aerosol layer (ATAL) domain  $(0-60^{\circ} \text{ E})$ . (b) The inter-annual variations of the average extinction coefficient in the upper troposphere (6-12 km), the ASR in the UTLS (13-18 km), and the vertical velocity at 100 hPa for the western ATAL domain  $(0-60^{\circ} \text{ E}, 25^{\circ} \text{ N})$ .

that aerosol particles have been transported into the upper troposphere region below 12 km altitude within the ASM anticyclone. This finding can explain the significant reduction of aerosols in the northern ASM region. Past studies showed that the aerosols transported into the lower stratosphere by the monsoon convection are confined within the strong anticyclonic circulation until breakup of the associated ASM anticyclone followed by recirculation in the lower stratosphere (Hoskins and Rodwell 1995, Highwood and Hoskins 1998, Fadnavis *et al* 2013, 2017). The asymmetry distribution of enhanced aerosols reveals a significant sink within the ASM region.

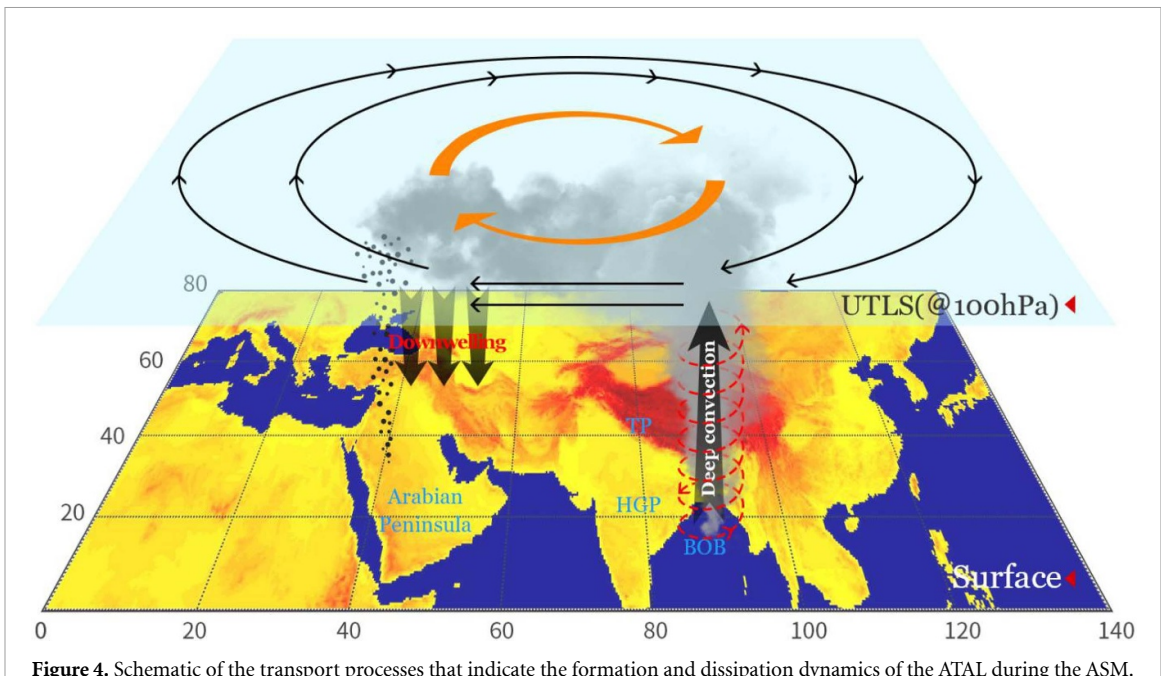


Figure 4. Schematic of the transport processes that indicate the formation and dissipation dynamics of the ATAL during the ASM.

We selected a vertical cross section at 0-60° E and 90° E of the western anticyclone to demonstrate the role of downward transport in this area, which plays a key role in balancing the ATAL intensity. For quantitative comparison, we calculated the average extinction coefficients in the upper troposphere (6–12 km) and the vertical velocity at 100 hPa, and the ASR in the UTLS at the vertical cross section. As shown in figure 3(b), there is a clear relationship between the vertical velocity and the upper tropospheric extinction coefficient. Attada et al (2019) confirmed that the impact of ASM on the Arabian climate is mainly associated with large-scale circulation variability in the upper troposphere through monsoon induced downward motion. The load of UTLS aerosols in the western anticyclone can also impact the concentration levels further downward through descending motion in the upper troposphere, as indicated by the similar inter-annual variation trends between the extinction coefficient and ASR for the years 2015-2018. However, their relationship is not significant for the period before 2015. Statistical analysis indicates that the correlation of the extinction coefficient with ASR does not meet the 95% confidence level of student t test (see table S2). A possible reason for this asynchronic variation is that the transport capacity of aerosols by descending motion approaches saturation for the abundant aerosol loading in the UTLS. But it is evident that the descending motion can play a role in the dissipation of the ATAL.

To summarize, figure 4 illustrates the horizontal movement of the aerosols within the anticyclone and the vertical transport pathways in the troposphere that balance the intensity of the ATAL during the ASM season. Deep convection over the BoB plays a dominant role in the vertical transport of aerosols from

the polluted boundary layer to the UTLS within the anticyclone, where they are transported westward by the equatorial easterly jet. At approximately 70° E the aerosol particles and precursor gases are partially removed from the UTLS by the large-scale descending motion, resulting in a concentration reduction in the western part of the ASM anticyclone. Our analysis indicates that in addition to the large-scale ascending circulation inside and eddy shedding at the margins of the anticyclone (Park et al 2007, Garny and Randel 2013, 2016), downward transport in the western part of the ASM anticyclone provides an important dynamical aerosol sink in the UTLS, which maintains a balance in the intensity of the ATAL.

# Data availability statement

Any data that support the findings of this study are included within the article.

All data that support the findings of this study are included within the article (and any supplementary information files).

# Acknowledgments

This study was supported jointly by the National Natural Science Foundation of China (Grant Nos. 91637101, 91837311 and 91537213).

# **Author contributions**

Qianshan He, Jianzhong Ma, and Xiangdong Zheng designed the study and drafted the paper. Yanyu Wang, Haizhen Mu, Tiantao Cheng, and Ruilian He contributed to data analysis and interpretation. Guan Huang and Dongwei Liu contributed to figure production. Qianshan He, Jianzhong Ma, Yuhang Wang, and Jos Lelieveld discussed further analysis and interpreted the results. All authors contributed to improve the manuscript.

## Conflict of interests

The authors declare no competing interests.

## References

- Attada R *et al* 2019 The role of the Indian summer monsoon variability on Arabian Peninsula summer climate *Clim. Dyn.* **52** 3389–404
- Baldwin M P *et al* 2001 The quasi-biennial oscillation *Rev. Geophys.* **39** 179–229
- Basha G et al 2020 Asian summer monsoon anticyclone: trends and variability Atmos. Chem. Phys. 20 6789–801
- Bergman J W et al 2012 Seasonal differences of vertical-transport efficiency in the tropical tropopause layer: on the interplay between tropical deep convection, largescale vertical ascent, and horizontal circulations J. Geophys. Res.: Atmos. 117 D05302
- Bergman J W, Fierli F, Jensen E J, Honomichl S and Pan L L 2013 Boundary layer sources for the Asian anticyclone: regional contributions to a vertical conduit *J. Geophys. Res.: Atmos.* 118 2560–75
- Bian J *et al* 2011 Tropospheric pollutant transport to the stratosphere by Asian summer monsoon *Chin. J. Atmos. Sci.* **35** 807–902
- Bian J et al 2020 Transport of Asian surface pollutants to the global stratosphere from the Tibetan Plateau region during the Asian summer monsoon *Natl Sci. Rev.* 516–533
- Chen B, Xu X D, Yang S and Zhao T L 2012 Climatological perspectives of air transport from atmospheric boundary layer to tropopause layer over Asian monsoon regions during boreal summer inferred from Lagrangian approach *Atmos. Chem. Phys.* 12 5827–39
- Collimore C C, Martin D W, Hitchman M H, Huesmann A and Waliser D E 2003 On the relationship between the QBO and tropical deep convection *J. Clim.* **16** 2552–68
- Dee D P et al 2011 The ERA-Interim reanalysis: configuration and performance of the data assimilation system Q. J. R. MeteoR. Soc. 137 553–97
- Dethof A, O'Neill A, Slingo J M and Smit H G J 1999 A mechanism for moistening the lower stratosphere involving the Asian summer monsoon Q. J. R. Meteorol. Soc. 125 1079–106
- Ding Q and Fu Q 2018 A warming tropical central Pacific dries the lower stratosphere *Clim. Dynam.* **50** 2813–27
- Fadnavis S, Roy C, Sabin T P, Ayantika D C and Ashok K 2017 Potential modulations of pre-monsoon aerosols during El Niño: impact on Indian summer monsoon Clim. Dynam. 49 2279–90
- Fadnavis S, Semeniuk K, Pozzoli L, Schultz M G, Ghude S D, Das S and Kakatkar R 2013 Transport of aerosols in to the UTLS and their impact on the Asian monsoon region as seen in a global model simulation *Atmos. Chem. Phys.* **13** 8771–86
- Fu R, Hu Y, Wright J S, Jiang J H, Dickinson R E, Chen M, Filipiak M, Read W G, Waters J W and Wu D L 2006 Short circuit of water vapor and polluted air to the global stratosphere by convective transport over the Tibetan Plateau Proc. Natl Acad. Sci. USA 103 5664–9
- Fueglistaler S *et al* 2009 Tropical tropopause layer *Rev. Geophys.* 47 RG1004
- Garny H and Randel W J 2013 Dynamic variability of the Asian monsoon anticyclone observed in potential vorticity and correlations with tracer distributions J. Geophys. Res.: Atmos. 118 13421–33

- Garny H and Randel W J 2016 Transport pathways from the Asian monsoon anticyclone to the stratosphere Atmos. Chem. Phys. 16 2703–18
- Gettelman A *et al* 2004 Impact of monsoon circulations on the upper troposphere and lower stratosphere *J. Geophys. Res.:* Atmos. **109** D22101
- Gottschaldt K D *et al* 2018 Dynamics and composition of the Asian summer monsoon anticyclone *Atmos. Chem. Phys.* **18** 5655–75
- Gu Y, Liao H and Bian J 2016 Summer time nitrate aerosol in the upper troposphere and lower stratosphere over the Tibetan Plateau and the South Asian summer monsoon region Atmos. Chem. Phys. 16 6641–63
- He Q, Ma J, Zheng X, Yan X, Vömel H, Wienhold F G, Gao W, Liu D, Shi G and Cheng T 2019 Observational evidence of particle hygroscopic growth in the upper troposphere–lower stratosphere (UTLS) over the Tibetan Plateau Atmos. Chem. Phys. 19 8399–406
- Highwood E J and Hoskins B J 1998 The tropical tropopause Q. J. R. MeteoR. Soc. 124 1579–604
- Höpfner M et al 2019 Ammonium nitrate particles formed in upper troposphere from ground ammonia sources during Asian monsoons Nat. Geosci. 12 608–12
- Höpfner M, Volkamer R, Grabowski U, Grutter M, Orphal J, Stiller G, von Clarmann T and Wetzel G 2016 First detection of ammonia (NH3) in the Asian summer monsoon upper troposphere Atmos. Chem. Phys. 16 14357–69
- Hoskins B J and Rodwell M J 1995 A model of the Asian summer monsoon. Part I: the global scale *J. Atmos. Sci.* **52** 1329–40
- Krishnamurti T N 1985 Summer monsoon experiment—a review *Mon. Weath. Rev.* **113** 1590–626
- Krotkov N A *et al* 2016 Aura OMI observations of regional SO<sub>2</sub> and NO<sub>2</sub> pollution changes from 2005 to 2015 *Atmos. Chem. Phys.* **16** 4605–29
- Lamotte C et al 2020 Modeling study of the impact of SO<sub>2</sub> volcanic passive emissions on the tropospheric sulfur budget Atmos. Chem. Phys. Discuss. 2020 1–41
- Lau K M and Li M T 1984 The monsoon of East Asia and its global associations—a survey B. Am. Meteorol. Soc. 65 114–25
- Lau WKM, Yuan C and Li Z 2018 Origin, maintenance and variability of the Asian Tropopause Aerosol Layer (ATAL): the roles of monsoon dynamics *Sci. Rep.* **8** 3960
- Lelieveld J et al 2018 The South Asian monsoon—pollution pump and purifier Science 6399
- Li Q et al 2005 Convective outflow of South Asian pollution: a global CTM simulation compared with EOS MLS observations *Geophys. Res. Lett* 32 L14826
- Luo J, Pan L L, Honomichl S B, Bergman J W, Randel W J, Francis G, Clerbaux C, George M, Liu X and Tian W 2018
  Space—time variability in UTLS chemical distribution in the Asian summer monsoon viewed by limb and nadir satellite sensors Atmos. Chem. Phys. 18 12511–30
- Ma J *et al* 2019 Modeling the aerosol chemical composition of the tropopause over the Tibetan Plateau during the Asian summer monsoon *Atmos. Chem. Phys.* **19** 11587–612
- Ming S, Wang W and Jin S 2019 Variability of temperature and ozone in the upper troposphere and lower stratosphere from multi-satellite observations and reanalysis data *Atmos*. *Chem. Phys.* **19** 6659–79
- Neely R R, Yu P, Rosenlof K H, Toon O B, Daniel J S, Solomon S and Miller H L 2014 The contribution of anthropogenic SO2 emissions to the Asian tropopause aerosol layer *J. Geophys. Res.: Atmos.* **119** 1571–9
- Nie J and Sobel A H 2015 Responses of tropical deep convection to the QBO: cloud-resolving simulations *J. Atmos. Sci.* 72 3625–38
- Nützel M, Dameris M and Garny H 2016 Movements, drivers and bimodality of the South Asian High *Atmos. Chem. Phys.* **16** 14755–74
- Pan L L *et al* 2016 Transport of chemical tracers from the boundary layer to stratosphere associated with the dynamics of the Asian summer monsoon *J. Geophys. Res.: Atmos.* 121 14159–74

- Park M et al 2009 Transport pathways of carbon monoxide in the Asian summer monsoon diagnosed from model of ozone and related tracers (MOZART) J. Geophys. Res.: Atmos. 114 D08303
- Park M, Randel W J, Emmons L K, Bernath P F, Walker K A and Boone C D 2008 Chemical isolation in the Asian monsoon anticyclone observed in Atmospheric Chemistry Experiment (ACE-FTS) data Atmos. Chem. Phys. 8 757–64
- Park M, Randel W J, Gettelman A, Massie S T and Jiang J H 2007 Transport above the Asian summer monsoon anticyclone inferred from aura microwave limb sounder tracers J. Geophys. Res.: Atmos. 112 D16309
- Plumb R A and Bell R C 1982 A model of the quasi-biennial oscillation on an equatorial beta-plane Q. J. R. Meteorol. Soc. 108 335–52
- Pokhrel S, Chaudhari H S, Saha S K, Dhakate A, Yadav R K, Salunke K, Mahapatra S and Rao S A 2012 ENSO, IOD and Indian Summer Monsoon in NCEP climate forecast system Clim. Dynam. 39 2143–65
- Randel W J and Park M 2006 Deep convective influence on the Asian summer monsoon anticyclone and associated tracer variability observed with atmospheric infrared sounder (AIRS) J. Geophys. Res.: Atmos. 111 D12314
- Randel W J, Park M, Emmons L, Kinnison D, Bernath P, Walker K A, Boone C and Pumphrey H 2010 Asian monsoon transport of pollution to the stratosphere *Science* 328 611–3
- Randel W J, Zhang K and Fu R 2015 What controls stratospheric water vapor in the NH summer monsoon regions? *J. Geophys. Res.: Atmos.* **120** 7988–8001
- Ravindrababu S, Ratnam M, Basha G, Liou Y-A and Reddy N 2019 Large anomalies in the tropical upper troposphere lower stratosphere (UTLS) trace gases observed during the extreme 2015–16 El Niño event by using satellite measurements *Remote Sens.* 11 687
- Renard J B, Dulac F, Durand P, Bourgeois Q, Denjean C, Vignelles D, Couté B, Jeannot M, Verdier N and Mallet M 2018 *In situ* measurements of desert dust particles above the western Mediterranean Sea with the balloon-borne light optical aerosol counter/sizer (LOAC) during the ChArMEx campaign of summer 2013 *Atmos. Chem. Phys.* 18 3677–99
- Schoeberl M R et al 2008 QBO and annual cycle variations in tropical lower stratosphere trace gases from HALOE and Aura MLS observations J. Geophys. Res.: Atmos. 113 D05301
- Srivastava A K, Misra A, Kanawade V P and Devara P C S 2016 Aerosol characteristics in the UTLS region: s satellite-based study over North India *Atmos. Environ.* 125 222–30
- Thomason L W and Vernier J-P 2013 Improved SAGE II cloud/aerosol categorization and observations of the Asian tropopause aerosol layer: 1989–2005 *Atmos. Chem. Phys.* 13 4605–16
- Tweedy O V, Kramarova N A, Strahan S E, Newman P A, Coy L,
  Randel W J, Park M, Waugh D W and Frith S M 2017
  Response of trace gases to the disrupted 2015–2016
  quasi-biennial oscillation Atmos. Chem. Phys. 17 6813–23
- Tzella A and Legras B 2011 A Lagrangian view of convective sources for transport of air across the Tropical Tropopause Layer: distribution, times and the radiative influence of clouds Atmos. Chem. Phys. 11 12517–34

- Vaughan M, Powell K A, Winker D M, Hostetler C A, Kuehn R E, Hunt W H, Getzewich B J, Young S A, Liu Z and Mcgill M J 2009 Fully automated detection of cloud and aerosol layers in the CALIPSO lidar measurements. *J. Atmos. Ocean. Tech.* 26 2034–50
- Vernier J-P et al 2011 CALIPSO detection of an Asian tropopause aerosol layer *Geophys. Res. Lett.* **38** L07804
- Vernier J-P *et al* 2018 BATAL: the balloon measurement campaigns of the Asian tropopause aerosol layer *Bull. Am. Meteorol. Soc.* **99** 955–73
- Vernier J-P, Fairlie T D, Natarajan M, Wienhold F G, Bian J, Martinsson B G, Crumeyrolle S, Thomason L W and Bedka K M 2015 Increase in upper tropospheric and lower stratospheric aerosol levels and its potential connection with Asian pollution *J. Geophys. Res.: Atmos.* 120 1608–19
- Vogel B, Günther G, Müller R, Grooß J-U, Hoor P, Krämer M, Müller S, Zahn A and Riese M 2014 Fast transport from Southeast Asia boundary layer sources to nothern Europe: rapid uplift in typhoons and eastward eddy shedding of the Asian monsoon anticyclone Atmos. Chem. Phys. 14 12745–62
- Webster P J et al 1998 Monsoons: processes, predictability and the prospects for prediction J. Geophys. Res.: Oceans. 103 14451–510
- Webster P J and Yang S 1992 Monsoon and ENSO: selectively interactive systems Q. J. R. MeteoR. Soc. 118 877–926
- Winker D M, Vaughan M A, Omar A, Hu Y, Powell K A, Liu Z, Hunt W H and Young S A 2009 Overview of the CALIPSO mission and CALIOP data processing algorithms *J. Atmos. Ocean. Tech.* **26** 2310–23
- Wright J S, Fu R, Fueglistaler S, Liu Y S and Zhang Y 2011 The influence of summertime convection over Southeast Asia on water vapor in the tropical stratosphere J. Geophys. Res.: Atmos. 116 D12302
- Wu G, Liu Y, Zhang Q, Duan A, Wang T, Wan R, Liu X, Li W, Wang Z and Liang X 2007 The influence of mechanical and thermal forcing by the Tibetan Plateau on Asian climate *J. Hydrometeor.* **8** 770–89
- Yan R C and Bian J C 2015 Tracing the boundary layer sources of carbon monoxide in the Asian summer monsoon anticyclone using WRF-Chem Adv. Atmos. Sci. 32 943–51
- Yan R C, Bian J C and Fan Q J 2011 The impact of the South Asia high bimodality on the chemical composition of the upper troposphere and lower stratosphere Atmos. Ocean. Sci. Lett. 4 229–34
- Yanai M, Li C and Song Z 1992 Seasonal heating of the Tibetan Plateau and its effects on the evolution of the Asian summer monsoon *J. Meteorol. Soc. Japan* **70** 319–51
- Yu P et al 2017 Efficient transport of tropospheric aerosol into the stratosphere via the Asian summer monsoon anticyclone Proc. Natl Acad. Sci. USA 114 6972–7
- Yu P, Toon O B, Neely R R, Martinsson B G and Brenninkmeijer C A M 2015 Composition and physical properties of the Asian tropopause aerosol layer and the North American tropospheric aerosol layer *Geophys. Res. Lett.* 42 2540–6
- Yuan C, Lau W K M, Li Z and Cribb M 2019 Relationship between Asian monsoon strength and transport of surface aerosols to the Asian Tropopause Aerosol Layer (ATAL): interannual variability and decadal changes Atmos. Chem. Phys. 19 1901–13